Effects of Acid Treatment of Pt–Ni Alloy Nanoparticles@Graphene on the Kinetics of the Oxygen Reduction Reaction in Acidic and Alkaline Solutions

ARTICLE *in* THE JOURNAL OF PHYSICAL CHEMISTRY C · DECEMBER 2010

Impact Factor: 4.77 · DOI: 10.1021/jp108305v

Effects of Acid Treatment of Pt−Ni Alloy Nanoparticles@Graphene on the Kinetics of the Oxygen Reduction Reaction in Acidic and Alkaline Solutions

Ke Zhang,[†] Qiaoli Yue,[†] Guifen Chen,[†] Yanling Zhai,[†] Lei Wang,[†] Huaisheng Wang,[†] Jinsheng Zhao,[†] Jifeng Liu,*[,†] Jianbo Jia,*[,‡] and Haibo Li*[,†,§]

Department of Chemistry, Liaocheng University, Liaocheng, 252059, Shandong, China, State Key Laboratory of Electroanalytical Chemistry, Changchun Institute of Applied Chemistry, Chinese Academy of Sciences, Changchun 130022, China, and Department of Chemistry, University of Science and Technology of China, Hefei, 230026, Anhui, China

Received: September 1, 2010; Revised Manuscript Received: November 8, 2010

Acidic dissolution of transition metals from Pt based alloy catalysts for oxygen reduction reaction (ORR) is an unavoidable process during fuel cell operation. In this work we studied the effect of acid treatment of graphene-supported Pt_1Ni_x($x = 0$, 0.25, 0.5, 1, and 2) alloys on the kinetics of the ORR in both alkaline and acidic solutions together with the generation of OH radicals in alkaline solutions. The alloy nanoparticles were synthesized through coimpregnation and chemical reduction. The electronic and structural features of the alloy were characterized by X-ray photoelectron spectroscopy, X-ray diffraction, transmission electron microscopy, and high-resolution transmission electron microscopy. The ORR performances were studied using cyclic voltammetry and rotating ring disk electrode techniques in 0.05 M H_2SO_4 and 0.1 M NaOH, respectively. The alloy catalysts were more active than pure Pt toward ORR, and after acid treatment the ORR activity of Pt−Ni alloy was enhanced in both acidic and alkaline media. The maximum activity of the Pt-based catalysts was found with ca. 50 atom % Ni content in the alloys (Pt_1Ni_1@graphene). OH radicals were generated through dissociation of hydroperoxide at the catalysts' surface and detected by fluorescence technique using terephthalic acid as capture reagent, which readily reacts with OH radical to produce highly fluorescent product, 2-hydroxyterephthalic acid. More OH radicals were found to be generated at Pt_1Ni_1@graphene catalyst. This work may be valuable in the design of electrocatalysts with higher ORR activity but lower efficiency of OH radical generation.

1. Introduction

The oxygen reduction reaction (ORR) plays an important role in fuel cells, such as polymer electrolyte fuel cells and proton exchange membrane fuel cells.[1] Electrocatalysts including nanoparticles (NPs), macrocycles and pyrolysis products, carbons, chalcogenides, enzymes, and coordination complexes have been reported for ORR use and reviewed recently.[1] Comparatively, among the reported electrocatalysts, NPs of platinum and platinum based alloy are the most widely used and studied catalysts. However, because of the high cost and low abundance of Pt, practical use and introduction of fuel cells into markets are limited. So the most critical challenges for the study and application of fuel cells have been to develop alternative electrocatalysts that will retain the high activity of Pt while lowering the cost.[2]

There are two possible ways to do this: make catalysts that use no Pt or make catalysts that use less Pt.[3] The non-Pt catalysts, such as non-platinum alloys,[4−7] nitride transition metal,[8−10] nitrogen-doped carbon materials including nitrogen-doped graphene,[2,11−17] metal oxides,[18−23] ruthenium-based chalcogenides,[24,25] pyrolyzed or metal porphyrins,[26−28] cobalt−polypyrrole composite,[29,30] enzymes,[31,32] polymers,[33] polymer composites,[34] or non-Pt based alloys[7] have been studied. However, their electrocatalytic activities are generally less than that of Pt.

To reduce the use of precious Pt in the catalysts of fuel cells, very low noble metal loading to form a monolayer supported on surfaces of single crystals,[35,36] or metal NPs[37−39] has been tried. Actually, the configuration of a Pt monolayer supported on NP is a "core−shell" structure.[37]

Another means of reducing the use of Pt is to use Pt based catalysts where Pt was alloyed with transition metals, such as Fe, Co, Ni, Cr, and Cu.[3,40−45] In particular, the Pt−Co alloy is the most widely used catalyst among Pt−M alloys because it is relatively easy to prepare. Usually there is dissolution of the transition metals from the Pt based alloys upon exposure to acids[46−50] and improved ORR activity in acidic media compared to pure Pt can be found,[3,46] and these have been ascribed to formation of a Pt skin at the surface of the alloy. Pt skin has optimum electronic structures, and the ORR activity decreases in the order: Pt skin > Pt skeleton > pure polycrystalline Pt. Latest studies showed that only surface atoms can go into solution and the amount of the leached transition metal ions did not exceed the maximal concentration of that at the alloy surface.[50] The thickness of a Pt-skin surface layer is usually less than 1 nm. The layer consists of only platinum atoms and is stable after immersion into an electrolyte.[51] When alloy catalysts are used, the dissolved metal ions sometimes are highly undesired because they could react with H_2O_2, an intermediate during ORR to generate hydroxyl (OH) radicals in acidic media through Fenton-like route,[49] thus causing accelerated degradation

* Corresponding authors: Jifeng Liu, liujifeng111@gmail.com; Jianbo Jia, jbjia@ciac.jl.cn; Haibo Li, haiboli@mail.ustc.edu.cn.
[†] Department of Chemistry, Liaocheng University.
[‡] State Key Laboratory of Electroanalytical Chemistry, Changchun Institute of Applied Chemistry.
[§] Department of Chemistry, University of Science and Technology of China.

10.1021/jp108305v
Published on Web 12/10/2010

of Nafion membrane and oxidation of the carbon support.[52,53] Recently efforts have been devoted to development of dissolution-resistant core−shell materials for acid medium ORR electrocatalysts.[54] However, leaching of transition metal atoms from the alloy surface is beneficial to prepare highly efficient catalysts.[50] Actually, acid treatment or dealloying has been used to fabricate nanoporous Au catalysts for methanol or CO oxidation.[55,56]

Comparatively, the studies of ORR activities on Pt alloys obtained in alkaline media are limited and there are discrepancies for reported results. For example, for Pt−Co alloys, different results have been reported. The alloy catalysts have lower,[57] similar,[58] slightly higher,[59] and higher[35,60] activities than the pure metal catalysts, and the reasons for the different results are not clear. The lower activity has been attributed to screening of Pt active sites by OH adsorbed on Co sites,[57] while the higher activity was explained based on optimal structural and electronic features consisting of optimum number of Pt coordination, Pt−Pt distance, and d-electron density in Pt or optimum d-band center energies.[35,60] In our previous work,[61] we studied ORR performance of Pt−Co alloy NPs supported on graphene. The alloy catalysts showed higher ORR activity than pure Pt catalysts in alkaline solutions while Pt_1Co_1 (atomic ratio) had the highest ORR activity. Generation of OH radicals has been found during ORR at alloy catalyst in alkaline solutions, and it has been explained as the dissociation of intermediate HO_2^- at the alloy surface.[61]

In this work, ORR activity of Pt−Ni alloy NPs supported on graphene was studied in both alkaline and acidic medium together with the generation of OH radicals in alkaline solution. Pt−Ni alloys have been reported to have improved ORR activity in acidic media as compared to pure Pt.[41,42,62,63] Graphene is regarded as a two-dimensional carbon material with huge specific surface and has recently been used in fuel cells as catalyst support.[64,65] Here, the graphene supported alloy NPs were fabricated through reducing mixed solutions of Pt and Ni ions using sodium borohydride ($NaBH_4$), and then the alloy NPs were treated using acid to remove the surface Ni atoms. The as-prepared alloy NPs were characterized by X-ray diffraction (XRD), X-ray photoelectron spectroscopy (XPS), transmission electron microscopy (TEM), and electrochemistry. The effects of acid treatment on ORR activity in acidic and alkaline solutions were studied. A dependence of ORR activity and OH radical generation upon composition of the alloy was found, and this work may be helpful for designing ORR catalysts.

2. Experimental Section

2.1. Chemicals and Apparatus. All chemicals used in this paper were at least analytical reagent grade, and water was prepared from a Milli-Q water purification system (≥18 MΩ). K_2PtCl_4 was purchased from Delan Fine Chemical Plant (Tianjin, China). $NiC_4H_6NiO_4 \cdot 6H_2O$ and $NaBH_4$ were obtained from Jingchun Chemical Reagent Co. (Shanghai, China). Terephthalic acid (TA) was purchased from Fluka Co. Flake graphite (300 mesh) was obtained from Kanglong Co. (Qingdao, China).

A Hitachi-800 TEM (coupled with a digital image system) was applied to observe the morphology of alloy NPs and the accelerating voltage was 150 kV. High-resolution transmission electron microscopy (HRTEM) images were obtained with a JEOL 2010 microscope at an acceleration voltage of 200 kV. Specimens were prepared for TEM by making suspensions of the catalyst powders in ethanol, using an ultrasonic bath. These suspensions were dropped onto clean polymer film or carbon-coated copper grid for TEM and HRTEM, respectively.

XRD measurements of Pt@graphene and Pt_1Ni_x@graphene were carried out on a Bruker D8 X-ray diffractometer using Cu Kα radiation ($\lambda = 0.15406$ nm). The sample containing ca. 10 mg of catalysts was deposited on a Si wafer cut along the(511) plane. The XRD spectra were obtained using high resolution in the step-scanning mode with a narrow receiving slit (0.4°) with a counting time of 5 s per 1°. Scans were recorded in the 2θ range of 10−90°. *d*-spacing(111) calculation was done using the program MDI Jade 5.0.

The electronic structures and surface compositions of the Pt and Pt−Ni alloy were performed on an ESCLAB MKII (VG Co., United Kingdom). The XPS data were collected with monochromatic Al Kα radiation. The binding energy scale of the spectra was aligned through the C(1s) peak at 284.6 eV. Peak fit analysis was done using the program XPS PEAK version 4.0.

Graphene oxide(GO) was obtained by oxidizing graphite using modified Hummer's method.[66] Briefly, graphite powder was mixed with strong oxidizing reagents such as potassium permanganate, concentrated sulfuric acid, hydrogen peroxide, and potassium persulfate. The mixture was sonicated and centrifuged and then was washed by water thoroughly. The dried GO powder was stored and dispersed in aqueous solution.

2.2. Preparation of Pt−Ni@Graphene. Weighted amounts of K_2PtCl_4 and $NiC_4H_6NiO_4 \cdot 6H_2O$ were added into GO solution (10 mL) to keep a fixed metal atomic ratio as Pt_1Ni_x, and the mixed solution of GO and metal ions was magnetically stirred and kept overnight. And then 10 mL of 20 mM freshly prepared $NaBH_4$ was added dropwise into the solution with stirring. During the addition of $NaBH_4$, a gradual color change to darkish was observed. After continuous stirring for 10 h, the resulted suspension was filtered and the catalyst was washed with copious water to remove halide ions. After drying at 80 °C, the graphene supported catalysts with 20% (wt) Pt−Ni alloy loading was obtained and denoted as Pt_1Ni_x@graphene and the atomic ratio was confirmed by energy dispersive X-ray (EDX) (atomic ratio, $x = 0$, 0.25, 0.5, 1, 2, respectively). In the acid treatment step, the prepared Pt_1Ni_x@graphene precursor powders were chemically dealloyed using mixed acids of 1 M H_2SO_4 and 1 M HNO_3 at 20 °C for 10 h under stirring, and followed by filtration, washing, and drying.

2.3. Electrochemical Measurements. Electrochemical measurements were conducted in a standard three-compartment electrochemical cell with a Pt wire and a saturated calomel electrode (SCE) used as the counter and the reference electrodes, respectively. The working electrodes were ordinary glassy carbon electrodes (GCs, 4 mm in diameter, Shanghai Chenhua Co.) or commercial rotating Pt ring-GC disk electrodes (RRDEs, 6.45 mm in diameter of disk, Jiangsu Jiangfen Electroanalytical Instrument Co. Ltd.). Ring and disk potential were controlled with a bipotentiostat CHI 832B electrochemical workstation (Shanghai Chenhua Co., China). The collection efficiency(*N*) of the ring electrode obtained by reducing potassium ferricyanide at the disk electrode is 0.497. Typically, the GC or RRDEs were polished using a 0.05 μm Al_2O_3 slurry and washed ultrasonically with ethanol and water separately. An aliquot of 4.0 μL (1 mg mL^{-1}) well-dispersed Pt_1Ni_x@graphene catalyst suspension was pipetted onto the GC disk using a microsyringe. After drying, 0.5 μL of 0.5 wt % Nafion (in ethanol) was placed immediately on the electrode surface to cover the graphene supported alloy catalyst. Nafion loading was very thin, within the range where the resulting Nafion diffusion limitation was considered to be negligible.[41,67] The electrolyte solution was 0.05 M H_2SO_4 or 0.1 M NaOH. The ORR measurements were carried out in the

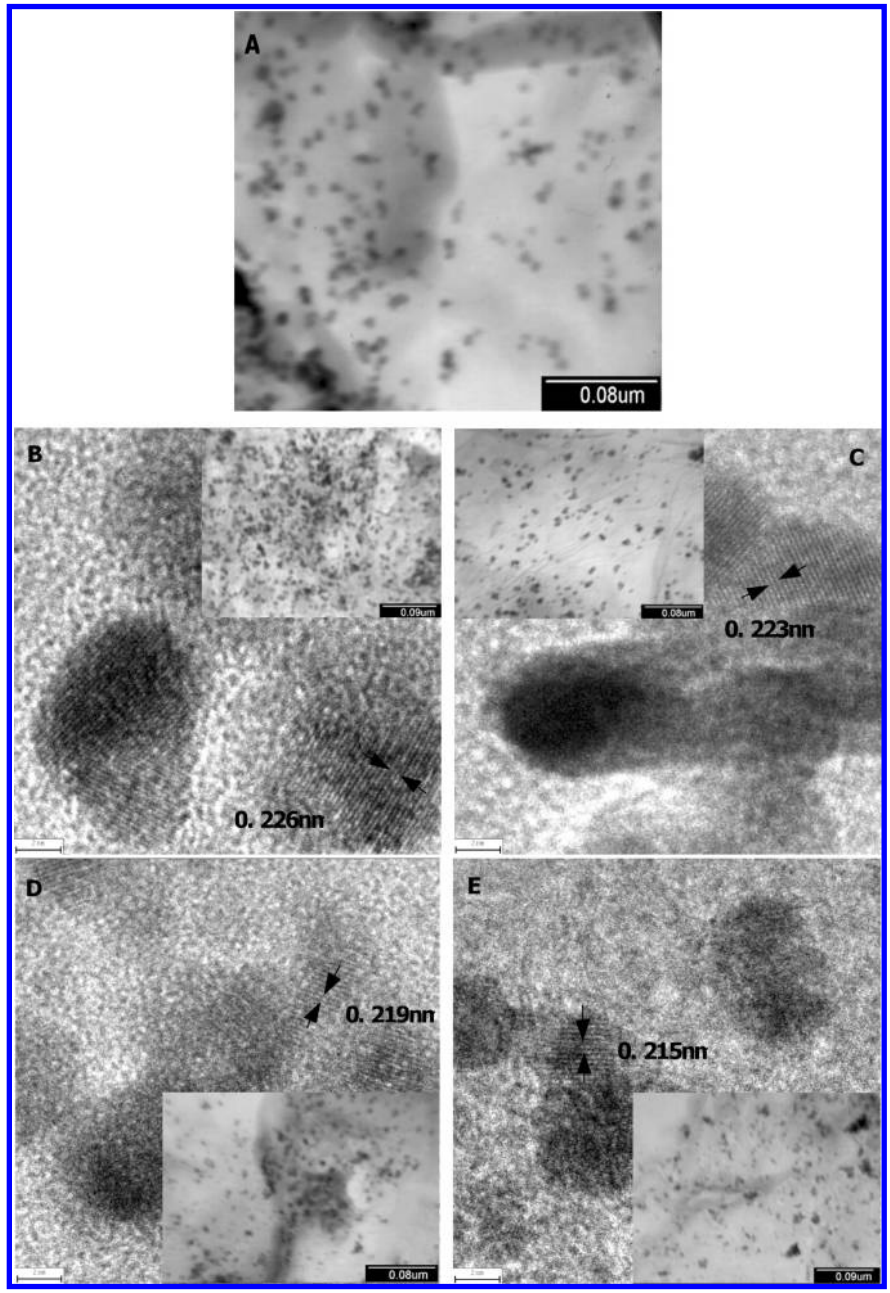

Figure 1. HRTEM micrographs of NPs samples: (A) Pt@graphene, (B) $Pt_1Ni_{0.25}$@graphene, (C) acid-treated $Pt_1Ni_{0.25}$@graphene, (D) Pt_1Ni_1@graphene, (E) acid-treated Pt_1Ni_1@graphene. Inset, TEM micrographs.

same solution, after saturating with air or O_2(>99.99%). All potentials in this work were given versus the SCE.

2.4. Detection of OH Radicals. The Pt_1Ni_x@graphene coated GC electrode was immersed in the mixing solution of 0.1 mM TA and 0.1 M NaOH. After being scanned with potential ranging from 0 to −1.0 V for 1500 cycles, the solution was transferred to an optical cell for fluorescence emission measurements. The fluorescence spectra of 2-hydroxyterephthalic acid (HTA), generated by the reaction of TA with the OH radicals produced in the ORR process, were measured using a Perkin-Elmer LS-50B fluorescence spectrometer. The excitation wavelength was 315 nm, and the emission peak was at 425 nm.

3. Results and Discussion

3.1. Catalyst Characterization. ***3.1.1. Pt−Ni Alloy Catalyst Morphology.*** The graphene-supported alloy catalysts were characterized by TEM and HRTEM. Low-magnification images (Figure 1) illustrate a highly dispersed and remarkably uniform catalyst (Pt_1Ni_x). All particles were considered to be spherical, and the resulting values of the diameter are summarized in Table 1 for catalysts with different Pt and Ni atomic ratios before and after acid treatments. The size distribution was uniform and the mean particle diameter was around 5−7 nm for all catalysts (Table 1). From the TEM, it was observed that the particle size decreased about 10% in diameter for the acid-treated alloy NPs, indicating that the Pt−Ni alloy was dissolved during acid treatment. The remained alloy NPs after acid treatment might be a structure of Pt skin and Pt skeleton beneath, and the surface was rich in Pt after Ni was dissolved into mixed acid of 1 M H_2SO_4 and HNO_3 at room temperature. It has been reported that the thickness of the Pt skin is less than 1 nm, the skin consists only of platinum atoms, and this structure is stable.[51]

The high-magnification HRTEM micrographs (Figure 1) show the dominant formation of face centered cubic (fcc) (111) lattice

TABLE 1: Physical Properties of the 20% Pt−Ni@Graphene Catalysts with Different Atomic Ratios

		Pt	acid-treated Pt_1Ni_1	acid-treated $Pt_1Ni_{0.25}$	acid-treated Pt_1Ni_2	Pt_1Ni_1	$Pt_1Ni_{0.25}$	Pt_1Ni_2
particle size (nm)	XRD[a]	6.1	5.3	4.9	4.7	4.7	5.1	6.2
	TEM[b]	7.0 ± 1.7	6.7 ± 2.2	7.4 ± 2.0	6.3 ± 2.4	6.4 ± 1.9	7.9 ± 1.7	7.1 ± 1.3
Pt(0) $4f_{7/2}$ (eV)		71.19	71.27	71.36	71.35	71.26	71.25	71.40
Pt(0) $4f_{5/2}$ (eV)		74.47	74.55	74.69	74.66	74.60	74.60	74.75
d-spacing[c] (nm)		0.227	0.218	0.223	0.219	0.221	0.225	0.219

[a] Mean particle diameter of the metal catalyst calculated by line broadening of powder. XRD peak using the Scherrer equation. [b] Mean particle diameter of the metal catalyst from TEM images. [c] *d*-spacing from XRD data(111).

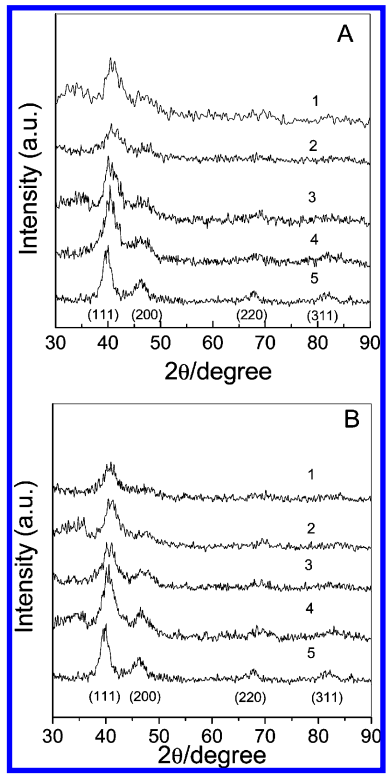

Figure 2. X-ray diffraction patterns (A) before acid treated and (B) acid treated, from catalysts: (1) Pt_1Ni_2@graphene, (2) Pt_1Ni_1@graphene, (3) $Pt_1Ni_{0.5}$@graphene, (4) $Pt_1Ni_{0.25}$@graphene, (5) Pt@graphene, respectively.

image of graphene-supported Pt−Ni. In comparison to the original Pt−Ni alloy NPs, the acid-treated NPs have rougher surface. The interplanar lattice of $Pt_1Ni_{0.25}$ catalyst was observed to be 0.226 nm, and the corresponding dealloyed PtNi NPs were observed to be 0.223 nm. These results are in good agreement with those obtained from *d*-spacing calculation from an X-ray diffraction pattern as shown in Table 1 (discussed below). After the alloy procedure, the phase of Pt−Ni was still dominated by Pt(111) and the interplanar distance of Pt−Ni alloy decreased slightly from that of pure Pt due to the interposition of Ni atoms into Pt(111).[64,68,69]

3.1.2. XRD Characterization. Figure 2 shows the XRD patterns of the garphene-supported Pt and Pt−Ni alloy catalysts with a metal loading of 20 wt % and different Pt/Ni atomic ratios. XRD clearly demonstrated the characteristic peaks of the Pt fcc structure with obvious peaks of Pt(111), but no characteristic peaks of Ni or its oxides were detected in Pt−Ni@graphene catalyst. Besides, an obvious higher angle shift of the Pt peak occurs for the alloy catalysts, indicating the formation of alloy of Pt and Ni.[42,70] After treatment with acid, the Pt(111) of Pt−Ni alloy NPs shifted slight positively to higher angle compared to alloy catalysts without acid treatment. Acid treatment may cause Ni atom dissolution and diffusion into solution and leave Pt skin structure, but some Ni ions may diffuse into Pt lattice of the Pt−Ni alloy beneath the Pt skin.[71]

The average size of the Pt−Ni alloy NPs was estimated by using the Scherrer equation[72]

$$d = \frac{k\lambda}{\beta_{1/2}\cos\theta} \tag{1a}$$

where d is the average particle diameter, k is a constant of 0.9, λ is the wavelength of the X-ray radiation (0.15406 nm), θ is the angle of the (220) peak, and $\beta_{1/2}$ is the peak width at half height. The average Pt−Ni alloy NPs sizes obtained for all the catalysts are given in Table 1, and the size values were in agreement with those obtained from TEM.

Both XRD and HRTEM results indicated that the geometric environment of the Pt NPs catalyst was changed by forming alloy with Ni, accompanied by a decrease in Pt−Pt bond distance as compared to that of pure Pt. The various Pt−Pt bond distance might have effects on ORR activities as reported.[73] A series of theories have been developed to discuss the catalytic ORR activity of Pt-based alloy nanostructured materials and the enhanced ORR activities have been ascribed to the following effects: rougher Pt surface and more active sites caused by dealloying transition metal;[47] change in the geometric structure of Pt (e.g., Pt−Pt bond distance and coordination number) and Pt 5d-orbital vacancies;[73−75] particle size or morphology effect;[76−78] decrease in the coverage of surface oxides and an enrichment of active Pt sites;[79] modification of the electronic structure of Pt and thus affecting the Pt−OH bond energetic.[80] However, based on theoretical studies, more and more works are now focused on effects of electronic structures (d-band model) caused by change in geometric or atomic configuration on ORR activities.[81] Recent studies on single crystalline thin films have revealed that the addition of Ni to Pt can change both the geometric and electronic structures of Pt.[82]

3.2. XPS Characterization. Figure 3A,B shows quick survey XPS spectra for the Pt−Ni alloy before and after the acid pretreatment. Both Pt and Ni are easily identifiable in the spectra, e.g., at 71/74 and 855/874 eV, respectively.[83] However, as shown in Figure 3B, the treatment in acidic media results in disappearance of the peaks characteristic of Ni, showing that Ni dissolution occurs during acid treatment. The electronic properties of Pt in Pt−Ni alloy were studied in detail and the XPS results are shown in Figure 3C. The spectra of Pt4f (Figure 3C, curve 2) was mutiply fitted with a mixed Gaussian−Lorentzian line shape. For $Pt_1Ni_{0.25}$@graphene, the Pt4f spectrum consisted of two peaks for metallic platinum at 71.25 (Pt $4f_{7/2}$) and 74.60 eV (Pt $4f_{5/2}$); with two more peaks at 72.12 and 75.44 eV, which could be assigned to Pt^{2+} species in PtO and $Pt(OH)_2$.[84] A comparison of the relative intensities of the peaks due to Pt(0) and those of PtO and $Pt(OH)_2$ showed that Pt in the PtNi NPs was predominately metallic.

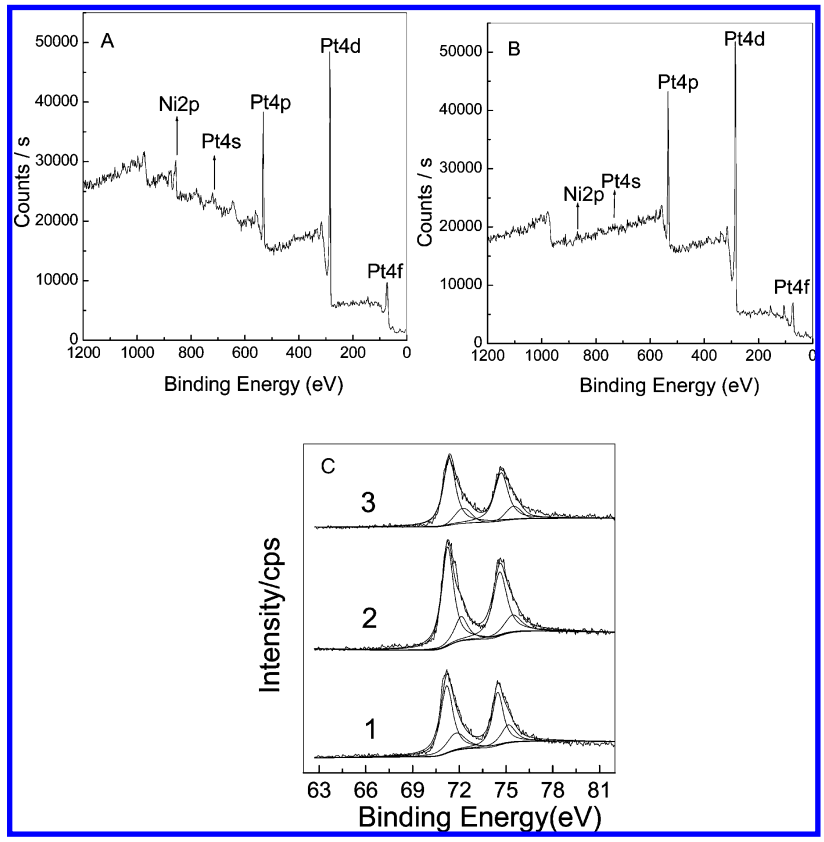

Figure 3. Representative XPS survey spectra for the PtNi alloy sample as-prepared Pt_1Ni_2@graphene (A) and after acid pretreatment (B). (C) XPS spectra of (1) Pt@graphene, (2) $Pt_1Ni_{0.25}$@graphene, (3) acid-treated $Pt_1Ni_{0.25}$@graphene.

Pt−Ni alloy positive shifts in the Pt 4f binding energy compared to values of pure Pt (Figure 3C, curve 2) suggested that the electronic structure of the Pt-skin layer is influenced by the Ni component in the underneath layer.[85] No XPS peaks of chloride were found, showing that the chloride ions were completely removed during washing. As shown in Figure 3C, the content of Pt(0) in $Pt_1Ni_{0.25}$@graphene (77.0%) is 7% more than that of pure Pt@graphene (70.8%). Acid treatment further increased the content of Pt(0) in $Pt_1Ni_{0.25}$@graphene to 81.9%. Higher content of Pt(0) in the alloy catalysts is beneficial to improving ORR electrocatalytic activity. A lightly positive shift Pt $4f_{5/2}$ binding energy was found for acid-treated Pt−Ni alloy (Figure 3C, curve 3 and Table 1).

Alloying with transition metals usually brings about chemical upshifts of binding energy for Pt skin and the bulk Pt−M alloy,[51] suggesting increased valence electron (5d) vacancy of the Pt in the electrode surface.[46,51,75,79] This change in electronic structure resulted in a strong metal−oxygen interaction; the upshifted binding energy after alloying will cause an increase of O_2^- (adsorbed) and O−O bond length and weakening of the O−O bond, resulting in fast ORR kinetics.[51]

3.3. Cyclic Voltammetry Study of Pt−Ni Alloy NP Modified Electrode. Figure 4A shows the cyclic voltammograms (CV) of the Pt@graphene and Pt_1Ni_1@graphene modified GC electrodes in 0.05 M H_2SO_4 degassed with Ar (>99.999%). The voltammetric features are similar. The adsorption and desorption of hydrogen within the potential range from −0.25 to 0.0 V, the double-layer capacitance region ranges between 0.0 and +0.5 V, the formation of Pt oxides at potentials more positive than +0.5 V, and the reduction of Pt oxides occurred in the cathodic potential scan. Such voltammetric features have been observed with other Pt based alloys such as Pt−Fe, Pt−Co, Pt−Ni, and Pt−V, and they have been ascribed to the formation of a "Pt skin" on the catalyst surface.[42,62,74,86,87]

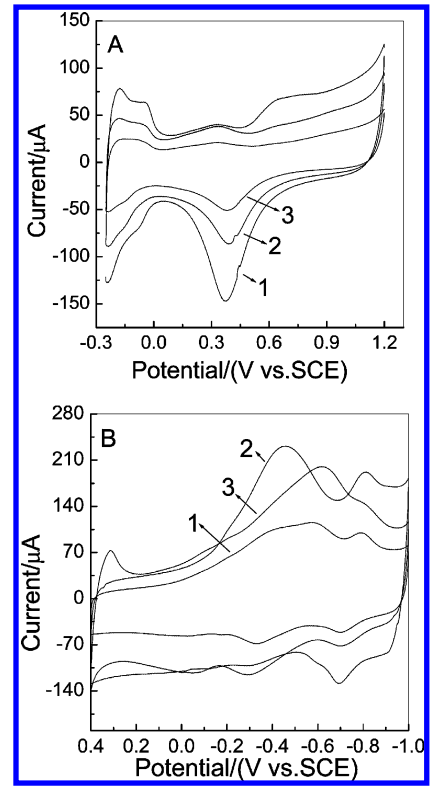

Figure 4. Cyclic voltammograms for the Pt and PtNi alloy electrode in (A) 0.05 M H_2SO_4 at 50 mV s^{-1} and (B) 0.1 M NaOH at 100 mV s^{-1}: (1) Pt@graphene, (2) acid treated Pt_1Ni_1@graphene, (3) Pt_1Ni_1@graphene.

A slight positive shift of the onset potential of oxide reduction peak was observed for alloy catalyst (Supporting Information,

TABLE 2: Kinetic Parameters for O_2 Reduction at Pt−Ni@Graphene/GC Electrodes in 0.05 M H_2SO_4

Catalysts	Q_H/mC	$E_{Pt\ oxides}$ (V)	E_{onset}/V	Tafel slop (mV/dec)	% H_2O_2[a]	n[b]	k^c (10^{-3})/ cm s^{-1}
Pt	0.164	0.477	0.50	−128	20.6	3.59	0.82
acid-treated Pt_1Ni_1	0.077	0.507	0.575	−113	14.7	3.71	2.50
acid-treated $Pt_1Ni_{0.25}$	0.103	0.503	0.574	−129	19.6	3.61	2.02
acid-treated Pt_1Ni_2	0.048	0.522	0.547	−119	16.4	3.67	1.92
Pt_1Ni_1	0.039	0.530	0.570	−129	19.6	3.61	2.02
$Pt_1Ni_{0.25}$	0.079	0.496	0.545	−109	18.3	3.71	1.96
Pt_1Ni_2	0.015	0.480	0.529	−112	17.2	3.61	1.61

[a] Potential was fixed at 0.15 V, calculated from eq 4a. [b] Calculated from eq 3a. [c] Potential was fixed at 0.36 V, calculated from eq 2c.

Figure S1) when compared to Pt@graphene. This positive shift can be attributed to the decrease of the desorption free energy($\triangle G_{ads}$) of Pt−OH, Pt−O, or Pt−O_2 species, due to the presence of the alloying element. This means that the adsorption strength of adsorbed oxygen species on Pt in the alloy is lower than that observed on pure Pt, so the reduction of ORR intermediates is more facile.[51]

The hydrogen underpotential deposition (H_{upd}) region of the alloys catalysts with Pt content lower than 50 atom % (atomic ratio) was nearly featureless, and the H_{upd} peaks typical for polycrystalline platinum were not resolved. However, after acid treatment, the shape of the H_{upd} region of the 50 atom % Pt catalyst was very similar to that of the pure Pt catalyst and showed the similar H-adsorption and desorption features in the potential region between 0 and −250 mV(Supporting Information, Figure S1). To determine the electrochemically active surface area, the H_{upd} region of different base voltammograms was integrated and the obtained H_{upd} charges are listed in Table 2 (column 1). As expected, the area in the H_{upd} region, i.e., the desorption pseudocapacitance, decreased with decreasing Pt content in the alloy. But acid treatment increased the H_{upd} region of alloy NPs or enlarged effective surface areas, thus enhancing the catalytic activity of ORR.

Figure 4B shows the results of CV measurements in 0.1 M air-saturated NaOH at Pt−Ni@graphene modified GC electrodes between 0.40 and −1.0 V, and they showed typical behavior regarding the hydrogen and the oxide regions of Pt@graphene and Pt−Ni@graphene in alkaline solutions.[58] Varying the Ni content had effects on both the ORR peak potential and the peak currents. The peak potential decreased with increasing Ni atomic ratio, but the peak currents increased with Ni content until 50 atom % Ni and then decreased for Pt_1Ni_2 alloy catalyst. We also found the acid-treated Pt−Ni NPs had much higher ORR peak current and lower onset potential.

3.4. Rotating-Ring Disk Electrode Voltammetry Study. The onset potential of ORR, the electrocatalytic activity, and the kinetics of ORR at the Pt−Ni alloy NPs were examined as functions of the catalyst composition and acid treatment using RRDE technique measurements.

The variation of ORR activity with alloy composition has been explained using d-band theory and the activity-d band center volcano dependences have been found for Pt monolayer on NP substrates,[36,87] single-crystal surfaces,[35,88] and polycrystalline alloy films (Pt_3M, M = Ni, Co, Fe, and Ti).[89] In our work, the potential of disk electrode was scanned from 0.9 to −0.2 V in 0.05 M H_2SO_4 and 0.2 to −1.0 V in 0.1 M NaOH with scan rate of 10 mV/s and the potential of ring electrode was controlled at 0.9 V in 0.05 M H_2SO_4 and 0.6 V in 0.1 M NaOH, so that the intermediate hydrogen peroxide produced during ORR at disk electrode can be reoxidized immediately at ring electrode.

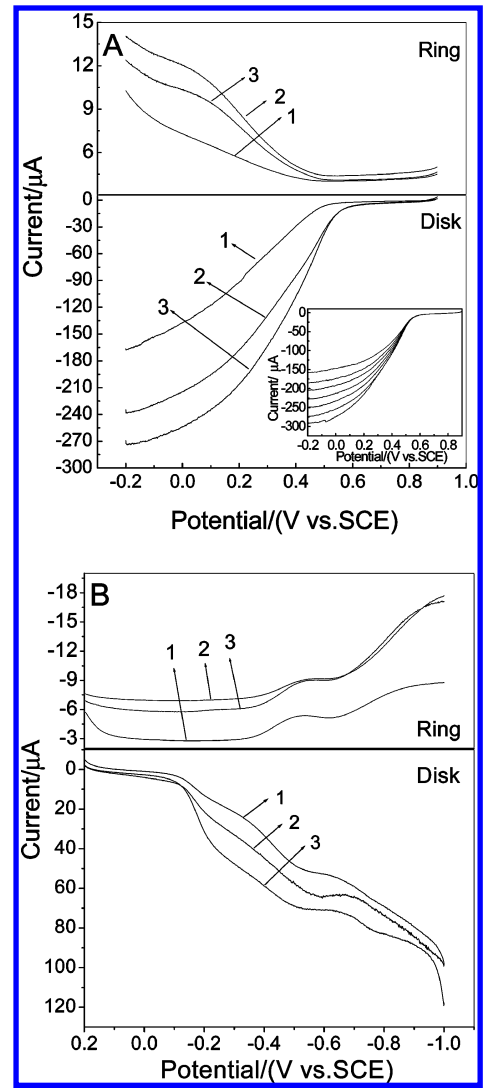

Figure 5. Current−potential curves for oxygen reduction on a Pt@graphene electrode (1), a PtNi@graphene alloy electrode (2), and a PtNi@graphene alloy electrode treated in acid (3). The samples were immobilized on a RRDE, and the measurements were carried out in (A) O_2-saturated 0.05 M H_2SO_4 and (B) 0.1 M air-saturated NaOH at 10 mV s^{-1} and 2000 rpm. Inset of top: RDE voltammograms for the Pt_1Ni_1@graphene alloy electrode treated in acid at different rotation rates.

Inset of Figure 5A shows steady-state polarization curves for the ORR in the disk modified with Pt_1Ni_1@graphene catalyst at various rotation speeds. It was observed that the ORR process at all catalysts was diffusion-controlled when the potential was smaller than 0.3 V and was under mixed kinetic-diffusion control in the potential region between 0.3 and 0.6 V. The ORR activity at alloy Pt−Ni catalysts was higher than that at pure Pt NPs in both alkaline and acidic medium. Acid treatment further increased the ORR activity of Pt−Ni alloy NPs catalysts, and this catalytic enhancement may be due to the formation of the Pt-skin structure at the surface of Pt−Ni NPs. The Pt skin causes a positive shift in the potential for OH_{ads} formation and makes more Pt active sites available for O_2 adsorption and reduction, which has been explained together with the upshifted binding energy by the d-band theory.[3,46,81,90] Similar results were obtained for the other catalysts with different atomic ratios as shown in Table 2, and the effects of composition on ORR activity were further studied.

The steady-state polarization curves for different acid treated Pt−Ni@graphene catalysts with different compositions at a

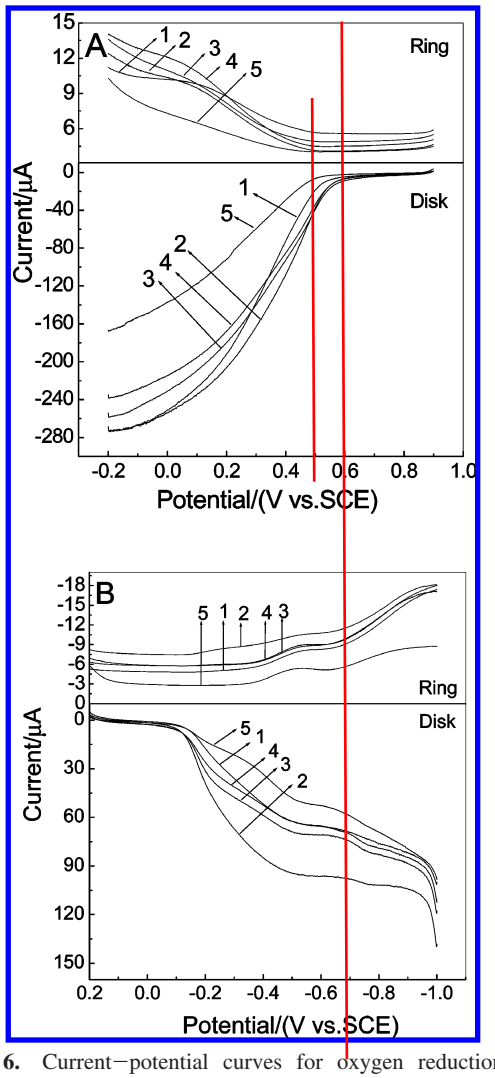

Figure 6. Current−potential curves for oxygen reduction on a Pt−Ni@graphene alloy electrode treated in acid. The samples were immobilized on a RRDE, and the measurements were carried out in (A) O_2-saturated 0.05 M H_2SO_4 and (B) 0.1 M air-saturated NaOH at 10 mV s^{-1} and 2000 rpm: (1) Pt_1Ni_2@graphene, (2) Pt_1Ni_1@graphene, (3) $Pt_1Ni_{0.5}$@graphene, (4) $Pt_1Ni_{0.25}$@graphene, (5) Pt@graphene, respectively.

rotation rate of 2000 rpm in 0.05 M H_2SO_4 are shown in Figure 6A. The onset potential of ORR of pure Pt catalyst is about 500 mV in 0.05 M H_2SO_4, whereas for Pt−Ni alloy catalysts, the onset potential shift positive to 574, 587, 575, and 547 mV for $Pt_1Ni_{0.25}$, $Pt_1Ni_{0.5}$, Pt_1Ni_1, and Pt_1Ni_2, respectively (Table 2). At the electrode potential of +0.20 V, the current density for the acid-treated alloy catalysts decreased in the order: −1.63 (Pt_1Ni_1) > −1.50 (Pt_1Ni_2) > −1.43 ($Pt_1Ni_{0.5}$) > −1.32 ($Pt_1Ni_{0.25}$) > −0.72 mA/cm^2 (Pt), respectively. So catalyst of Pt_1Ni_1@graphene gave the highest current density and had the lowest onset potential of ORR. Koutecky−Levich plots are compared in Figure 7.

Compared with commercial Vulcan XC-72 carbon, PtNi catalysts supported on graphene were more active than PtNi on Vulcan XC-72 carbon toward ORR in both acidic and alkaline media (Figure S2 in the Supporting Information). The ORR mass activities of PtNi alloy obtained from reported works are listed in the Supporting Information (Table S1). Comparatively, the ORR activities of PtNi@graphene used in our work were comparable to or higher than the reported results.

Figure 6B shows disk current of ORR at the Pt_1Ni_x@graphene modified GC electrode at a rotation rate of 2000 rpm in 0.1 M

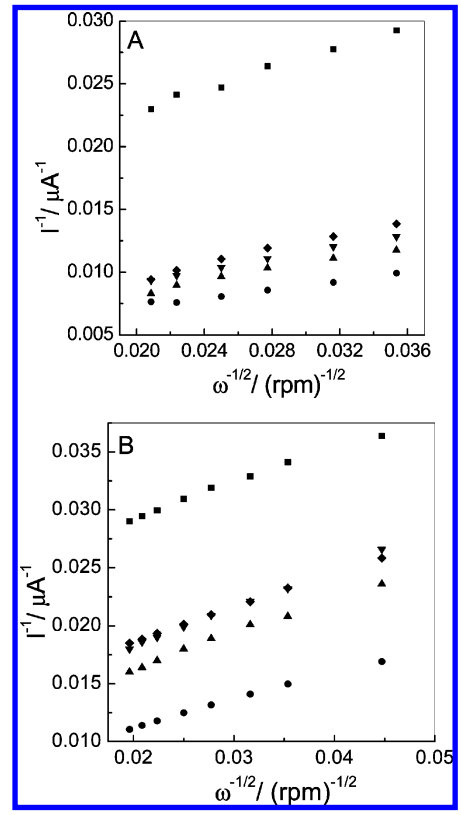

Figure 7. Comparison of Koutecky−Levich plots for the reduction of oxygen in 0.05 mol L^{-1} oxygen-saturated H_2SO_4 solution and 0.1 mol L^{-1} air-saturated NaOH solution at GCE modified Pt_1Ni_x@graphene with different metal atomic ratios. The potential was fixed at 0.36 V and −0.4 V: ■, Pt; ●, acid-treated Pt_1Ni_1; ▼, acid-treated $Pt_1Ni_{0.25}$; ▲, acid-treated $Pt_1Ni_{0.5}$; ♦, acid-treated Pt_1Ni_2.

NaOH. ORR showed a two-step process with the onset potentials at about −0.15 and −0.65 V, respectively, for acid-treated Pt−Ni alloy catalysts with different atomic ratios. Obviously, the ORR current increased with increasing Pt:Ni atomic ratios from 1:0.25 to 1:1 and then decreased for Pt_1Ni_2. The different ORR activities of Pt−Ni catalysts were further plotted in Tafel curves as shown in Figure 8. At the same potential, the current decreased in the order Pt_1Ni_1 > $Pt_1Ni_{0.5}$ > $Pt_1Ni_{0.25}$ > Pt_1Ni_2 > pure Pt. The variation of the current with the particle composition obtained from RRDE was similar to that observed in CV.

Different magnitudes of the ring and disk currents for the ORR at Pt_1Ni_x@graphene showed that ORR involves the different number of electrons, and the corresponding parameters of the electrochemical ORR at bare Pt−Ni alloy catalysts can be obtained from the Koutecky−Levich plots (Figure 7)

$$\frac{1}{i} = \frac{1}{i_k} + \frac{1}{i_{l,c}} = \frac{1}{i_k} + \frac{1}{0.62nFAD_O^{2/3}\omega^{1/2}\nu^{-1/6}C_{O_2}^*} \quad (2a)$$

$$B = 0.62nFAD_O^{2/3}\omega^{1/2}\nu^{-1/6}C_{O_2}^* \quad (2b)$$

$$i_k = nFAkC_{O_2}^* \quad (2c)$$

where i represents the measured current, i_k is the kinetic current, $i_{l,c}$ is the limited current, n is the number of electron transfer, F is the Faraday constant, A is the geometric area of the GC disk, D_O is the diffusion coefficient of O_2, ω is the rotation rate, ν is

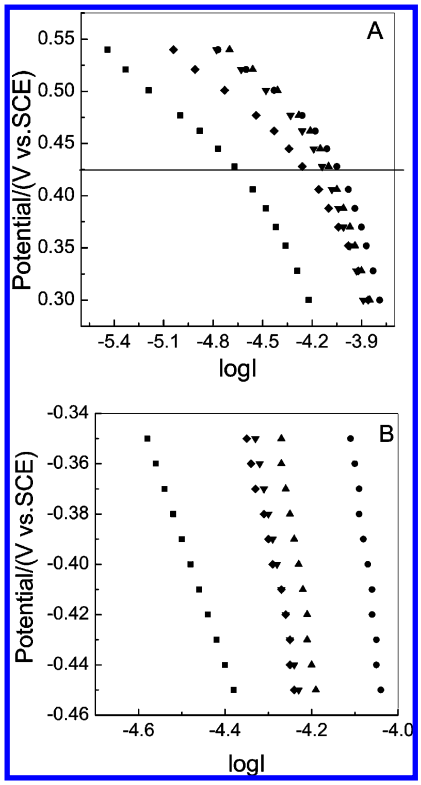

Figure 8. Tafel plots for Pt@graphene and Pt−Ni@graphene catalysts obtained using data from RRDE (2000 rpm) (A) 0.05 M H_2SO_4, (B) 0.1 M NaOH: ■, Pt; ●, acid-treated Pt_1Ni_1; ▼, acid-treated $Pt_1Ni_{0.25}$; ▲, acid-treated $Pt_1Ni_{0.5}$; ◆, acid-treated Pt_1Ni_2.

TABLE 3: Kinetic Parameters for O_2 Reduction at Pt−Ni@Graphene/GC Electrodes in 0.1 M NaOH

catalysts	E_{onset}/V	E_p/V	Tafel slope (mV/dec)	% HO_2^{-a}	n^b	k^c (10^{-3})/ cm s^{-1}
Pt	−0.126	−0.572	−500	36.2	3.27	3.6
acid-treated Pt_1Ni_1	−0.110	−0.457	−1430	36.0	3.28	9.3
acid-treated $Pt_1Ni_{0.25}$	−0.112	−0.384	−1000	42.5	3.19	5.8
acid-treated Pt_1Ni_2	−0.120	−0.440	−842	39.8	3.25	5.6
Pt_1Ni_1	−0.118	−0.618	−750	49.9	2.93	5.5
$Pt_1Ni_{0.25}$	−0.121	−0.594	−814	46.6	3.00	4.9
Pt_1Ni_2	−0.123	−0.579	−958	44.1	3.07	4.7

[a] Potential was fixed at −0.5 V, calculated from eq 4a. [b] Calculated from eq 3a. [c] Potential was fixed at −0.4 V, calculated from eq 2c.

the kinetic viscosity of the solution, and C_{O_2}* is the concentration of dissolved O_2 in solution. So the plots of i^{-1} vs $\omega^{-1/2}$ are anticipated to yield straight lines with the intercept corresponding to i_k (eq 2c) and the slopes reflecting the so-called B factors (eq 2b). The number of electrons per oxygen molecule (n) were obtained from the following equation

$$n = \frac{4I_D}{I_D + (I_R/N)} \tag{3a}$$

where N is the collection efficiency of the ring, I_D is the disk current, and I_R is the ring current. These results are listed in Tables 2 and 3 for all catalysts operated in acidic and alkaline solutions. In acidic solutions, the electron transfer showed no obvious change for acid-treated Pt−Ni alloy catalysts. While in alkaline media, the electron transfer values increased slightly for acid-treated alloy catalysts and were close to that of pure Pt catalysts(n = 3.27).

According to Koutecky−Levich plots (Figure 7) and the intercepts ($1/i_k$), the reaction rate constants (k) can be obtained quantitatively and are shown in Tables 2 and 3. Usually, Pt_1Ni_1@graphene had the fastest ORR kinetics.

A calculation of H_2O_2 percentage at a disk electrode was done according to the equation[91]

$$\% H_2O_2 = \frac{2I_R/N}{I_D + I_R/N} \tag{4a}$$

and the percentage of H_2O_2 generated at the disk is listed in Tables 2 and 3.

In 0.05 M H_2SO_4, the ring currents continuously increased starting from the potentials below 0.45 V. The percentage values of H_2O_2 production at all Pt−Ni alloy catalysts were roughly similar but lower than that on pure Pt. However, H_2O_2 production decreased for alloy catalysts with acidic treatment, especially Pt_1Ni_1@graphene decreased from 19.6% to 14.7% after acid treatment. Comparatively, the reported values of H_2O_2 yield obtained from Pt−Ni[73] and polycrystalline Pt_3Ni catalyst[80] are higher than Pt−Ni@graphene studied in this work. The yield of H_2O_2 is related to the loading of metal catalysts. Inaba et al. reported an increased H_2O_2 production with decreasing Pt loading,[92] and these observations are in agreement with studies on ORR using Pt−Co−Mn,[93] Ru[94] catalysts. When the density of catalytic site density is low, i.e., the sites for oxygen reducing are sparsely distributed, there is a higher tendency for the H_2O_2 molecules to escape further reduction to H_2O.

In 0.1 M NaOH, graphene is known to carry many oxygen-containing groups such as quinols, which facilitates generation of HO_2^- during ORR, and HO_2^- is the main product.[95−98] Our results agreed with the occurrence of the participation of the carbon substrates in the electrocatalytic ORR following the two-electrons mechanism and the four-electrons mechanism at the metal sites, that is

$$O_2 + 2e + H_2O \rightarrow HO_2^- \text{ (graphene)} \tag{5a}$$

$$O_2 + 4e + 2H_2O \rightarrow 4OH^- \text{ (platinum)} \tag{5b}$$

High percentage of HO_2^- was observed at Pt−Ni@graphene as shown in Table 3. However, after acid treatment, the alloy catalysts gave lower percentage of HO_2^-. For Pt_1Ni_1@graphene, HO_2^- yield decreased from 49.9% to 36% after acid treatment. Percentage of HO_2^- has been reported to be less than 7% for thin film porous Pt catalyst (10 wt % Pt loading) and less HO_2^- generated at higher Pt loading in alkaline solutions. The high percentage of HO_2^- may be due to the graphene supports. However, the ORR activity and HO_2^- yield of blank graphene support showed no obvious change after acid treatment (Figure S3 in the Supporting Information). So the change of HO_2^- yield of PtNi@graphene after acid treatment was due to the change of PtNi alloy.

Tafel plots for the pure Pt and Pt−Ni alloy catalysts are shown in Figure 8, where the overall shapes and slopes are different, and this implied that the ORR follows the different mechanism on the different catalysts in different media. The Tafel plot (Figure 8A) for the ORR in 0.05 M H_2SO_4 indicates that the Tafel slope is −120 mV dec^{-1} in the potential region above 0.425 V, with a transition to a very high value(<−350 mV dec^{-1}) below that. The Tafel slope of −120 mV dec^{-1} indicates that at low overpotentials the rate-determining step

SCHEME 1: The OH Radicals Generated in the ORR Process Can Be Quantified by Fluorescent Intensity of 2-HTA

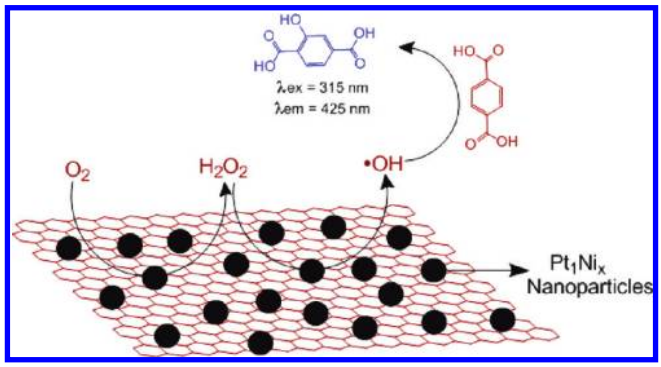

(rds) is the first charge transfer step.[14,99] Considering that a significant change in the Tafel slope usually implies a change in the rds, the transition in the Tafel slope below 0.425 V may represent a change in the rds. The Tafel plot (Figure 8B) shows the ORR in 0.1 M NaOH. It should be noted here that the Tafel slope values (<-500 mVdec^{-1}) were much higher than -120 mV. Such a variation of the slope in the Tafel plot has been attributed to the chemical steps including variation of the adsorption of the reaction intermediates (OH^-) and other specifically adsorbed species affecting the adsorption of the O_2 molecules.[51,74,100,101] In comparison, the rds for ORR at metal catalyst in acidic media is usually the electrochemical process where O_2 was reduced to form superoxide anion.

3.5. Generation of OH Radicals during ORR. The prepared GC was immersed in the mixing solution of 0.1 mM TA and 0.1 M NaOH. After being scanned with potential ranging from 0 to -1.0 V for 1500 cycles, the solution was transferred to an optical cell for fluorescence emission measurements. As shown in the scheme, TA can trap OH radicals to form 2-HTA (Scheme 1), which is a fluorophore ($\lambda_{ex} = 315$ nm, $\lambda_{em} = 425$ nm). So the OH radicals generated in the ORR process can be quantified by fluorescent intensity of 2-HTA.

This method has been used to detect OH radicals generated in TiO_2 photocatalytic reactions.[102−104] Liu and Girault et al. have studied the generation of OH radicals during ORR at Pd/ITO electrodes in neutral solutions,[105] during ORR at graphene supported Pt−Co alloy catalysts.[61] Here, this technique was used to detect OH radicals generated in ORR at Pt−Ni alloy catalysts. A dependence and generation of OH radicals upon the composition of Pt−Ni alloy electrocatalyst supported on graphene were found and illustrated in Figure 9. Pt_1Ni_1 had the highest yield of OH radicals compared to the alloy NPs with different composition. Acid treatment increased generation of OH radicals during ORR in alkaline solutions. Recently, we have studied ORR at graphene-supported Pt−Co alloy catalysts in 0.1 M NaOH.[61] Generation of OH radicals has been ascribed to the dissociation of intermediate hydrogen peroxide at surface transition metal oxide and Pt sites. Herein, with increasing Ni content the fluorescence increased and this may be due to both more H_2O_2 generation and more catalytic sites at alloy surface for peroxide dissociation to give OH radicals. At higher Ni content, e.g., Pt_1Ni_2, fewer OH radicals were produced and this may be caused by less H_2O_2 and less sites for production of OH radicals. After acid treatment, fluorescence increased and this may be due to more sites produced at the Pt-skin structure after dissolution of Ni during acid treatment.

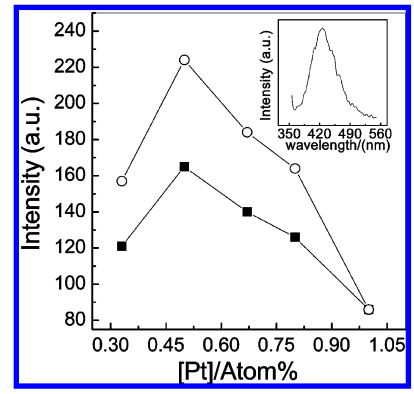

Figure 9. The effect of Pt:Ni atomic ratio on the fluorescence intensity. Inset, typical fluorescence spectra of 0.1 mM terephthalic acid with Pt−Ni@graphene/GC immersed in air-saturated 0.1 M NaOH solution with an applied potential ranging from 0 to -1.0 V after 1500 cycles (500 mV/s): ○, acid-treated PtNi; □, PtNi.

Conclusions

ORR at acid-treated graphene-supported Pt−Ni alloy NPs was studied, and the alloy catalysts had higher ORR activity than that at pure Pt catalysts in both acidic and alkaline solutions. The Pt−Ni alloy NPs were spherical and the size decreased slightly after acid treatment because of the dissolution of Ni atoms. The binding energy of Pt upshifted after alloying and upshifted more after acid treatment. These changes in geometric and electronic structure were beneficial for ORR. An interesting order of ORR was found: acid-treated Pt−Ni alloy > Pt−Ni alloy > Pt for both in acidic and alkaline solutions, and among the alloy catalysts with various atomic ratios Pt_1Ni_1@graphene had the highest activity. The percentage of hydrogen peroxide was less than 20% during ORR in 0.05 M H_2SO_4, while it ranged from 36% to 50% for ORR in 0.1 M NaOH. Graphene as a support may have facilitated 2e route to generate hydrogen peroxide. However, acid-treated Pt−Ni decreased yield of hydrogen peroxide in alkaline media. The intermediate peroxide dissociated at the alloy surface to generate OH radicals in alkaline solutions, and Pt_1Ni_1@graphene gave the highest quantity of OH radicals. So our studies suggest the following:

I. Acidic dissolution of alloyed transition metals is an unavoidable process during fuel cell operations, but now it can be used as a procedure (called acid treatment) to prepare alloy catalysts with higher activity in acidic and alkaline solutions.

II. The Pt_1Ni_1@graphene might represent an optimal composition for ORR among the catalysts with various atomic ratios under the present study because of the higher ORR activity and lower peroxide yield, but it gave more OH radicals.

This study may be helpful to designing ORR alloy catalysts with higher activity but lower yield of peroxide or OH radicals, because the reactive oxygen species are detrimental to the membrane electrode assembly of fuel cells.

Acknowledgment. J.L. and Q.Y. thank the Natural Science Foundation of China for Funding (21075058, 21005036, 20875042). J.J. and J.Z. thank Natural Science Foundation of China for Funding (20805044, 20906043). This work was also supported by the Higher Educational Science and Technology Program of Shandong (J10LB12), Key Project of Natural Science Foundation (ZR2010BZ004, 2010GJC20808-15), and the Tai-Shan Scholar Research Fund of Shandong Province.

Supporting Information Available: Cyclic voltammograms of Pt and PtNi alloy electrode in 0.05 M H_2SO_4 at 50 mV s^{-1},

RRDE voltammograms of Pt_1Ni_1@Vulcan XC-72, Pt_1Ni_1@graphene, and comparison of ORR mass activities of PtNi alloy reported previously with PtNi@graphene used in this study. This material is available free of charge via the Internet at http://pubs.acs.org.

References and Notes

(1) Gewirth, A. A.; Thorum, M. S. *Inorg. Chem.* **2010**, *49*, 3557.

(2) Kundu, S.; Nagaiah, T. C.; Xia, W.; Wang, Y.; Dommele, S. V.; Bitter, J. H.; Santa, M.; Grundmeier, G.; Bron, M.; Schuhmann, W.; Muhler, M. *J. Phys. Chem. C* **2009**, *113*, 14302.

(3) Duong, H. T.; Rigsby, M. A.; Zhou, W. P.; Wieckowski, A. *J. Phys. Chem. C* **2007**, *111*, 13460.

(4) Guo, J.; Hsu, A.; Chu, D.; Chen, R. *J. Phys. Chem. C* **2010**, *114*, 4324.

(5) Raghuveer, V.; Manthiram, A.; Bard, A. J. *J. Phys. Chem. B* **2005**, *109*, 22909.

(6) Fernandez, J. L.; Raghuveer, V.; Manthiram, A.; Bard, A. J. *J. Am. Chem. Soc.* **2005**, *127*, 13100.

(7) Yu, T. H.; Sha, Y.; Merinov, B. V.; Goddard, W. A. *J. Phys. Chem. C* **2010**, *114*, 11527.

(8) Jaouen, F. *J. Phys. Chem. C* **2009**, *113*, 15433.

(9) Jaouen, F.; Dodelet, J.-P. *J. Phys. Chem. C* **2009**, *113*, 15422.

(10) Jaouen, F.; Dodelet, J.-P. *Electrochim. Acta* **2007**, *52*, 5975.

(11) Qu, L.; Liu, Y.; Baek, J.-B.; Dai, L. *ACS Nano* **2010**, *4*, 1321.

(12) Ikeda, T.; Boero, M.; Huang, S.-F.; Terakura, K.; Oshima, M. Ozaki, J.-i. *J. Phy. Chem. C* **2008**, *112*, 14706.

(13) Kurak, K. A.; Anderson, A. B. *J. Phys. Chem. C* **2009**, *113*, 6730.

(14) Maldonado, S.; Stevenson, K. J. *J. Phys. Chem. B* **2005**, *109*, 4707.

(15) Thomas, A.; Fischer, A.; Goettmann, F.; Antonietti, M.; Muller, J.-O.; Schlogl, R.; Carlsson, J. M. *J. Mater. Chem.* **2008**, *18*, 4893.

(16) Lyth, S. M.; Nabae, Y.; Moriya, S.; Kuroki, S.; Kakimoto, M.-a.; Ozaki, J.-i.; Miyata, S. *J. Phys. Chem. C* **2009**, *113*, 20148.

(17) Chen, Z.; Higgins, D.; Tao, H.; Hsu, R. S.; Chen, Z. *J. Phys. Chem. C* **2009**, *113*, 21008.

(18) Cheng, F.; Su, Y.; Liang, J.; Tao, Z.; Chen, J. *Chem. Mater.* **2010**, *22*, 898.

(19) Roche, I.; Chainet, E.; Chatenet, M.; Vondrak, J. *J. Phys. Chem. C* **2007**, *111*, 1434.

(20) Adler, S. B. *Chem. Rev.* **2004**, *104*, 4791.

(21) Prakash, J.; Tryk, D. A.; Aldred, W.; Yeager, E. B. *J. Appl. Electrochem. Comm.* **1999**, *29*, 1463.

(22) Cheng, F.; Shen, J.; Ji, W.; Tao, Z.; Chen, J. *ACS Appl. Mater. Interfaces* **2009**, *1*, 460.

(23) Mao, L.; Zhang, D.; Sotomura, T.; Nakatsu, K.; Koshiba, N.; Ohsaka, T. *Electrochim. Acta* **2003**, *48*, 1015.

(24) Vante, N. A.; Tributsch, H. *Nature* **1986**, *323*, 431.

(25) Cao, D. X.; Wieckowski, A.; Inukai, J.; Alonso-Vante, N. *J. Electrochem. Soc.* **2006**, *153*, 869.

(26) Chen, W.; Akhigbe, J.; Bruckner, C.; Li, C. M.; Lei, Y. *J. Phys. Chem. C* **2010**, *114*, 8633.

(27) Fournier, J.; Lalande, G.; Cote, R.; Guay, D.; Dodelet, J.-P. *J. Electrochem. Soc.* **1997**, *144*, 218.

(28) Gojkovic, S. L.; Gupta, S.; Savinell, R. F. *J. Electroanal. Chem.* **1999**, *462*, 63.

(29) Bashyam, R.; Zelenay, P. *Nature* **2006**, *443*, 63.

(30) Zhou, Q.; Li, C. M.; Li, J.; Cui, X. Q.; Gervasio, D. *J. Phys. Chem. C* **2007**, *111*, 11216.

(31) Mano, N.; Fernandez, J. L.; Kim, Y.; Shin, W.; Bard, A. J.; Heller, A. *J. Am. Chem. Soc.* **2003**, *125*, 15290.

(32) Fei, J. F.; Song, H. K.; Tayhas, G.; Palmore, R. *Chem. Mater.* **2007**, *19*, 1565.

(33) Kingsborough, R. P.; Swager, T. M. *Chem. Mater.* **2000**, *12*, 872.

(34) Gajendran, P.; Saraswathi, R. *J. Phys. Chem. C* **2007**, *111*, 11320.

(35) Lima, F. H. B.; Zhang, J.; Shao, M. H.; Sasaki, K.; Vukmirovic, M. B.; Ticianelli, E. A.; Adzic, R. R. *J. Phys. Chem. C* **2007**, *111*, 404.

(36) Zhang, J.; Mo, Y.; Vukmirovic, M. B.; Klie, R.; Sasaki, K.; Adzic, R. R. *J. Phys. Chem. B* **2004**, *108*, 10955.

(37) Zhang, J.; Lima, F. H. B.; Shao, M. H.; Sasaki, K.; Wang, J. X.; Hanson, J.; Adzic, R. R. *J. Phys. Chem. B* **2005**, *109*, 22701.

(38) Guo, S.; Dong, S.; Wang, E. *J. Phys. Chem. C* **2009**, *113*, 5485.

(39) Guo, S. J.; Dong, S. J.; Wang, E. K. *J. Phys. Chem. C* **2008**, *112*, 2389.

(40) Lai, F.; Sarma, L. S.; Chou, H.; Liu, D.; Hsieh, C.; Lee, J.; Hwang, B. *J. Phys. Chem. C* **2009**, *113*, 12674.

(41) Paulus, U. A.; Wokaun, A.; Scherer, G. G.; Schmidt, T. J.; Stamenkovic, V.; Radmilovic, V.; Markovic, N. M.; Ross, P. N. *J. Phys. Chem. B* **2002**, *106*, 4181.

(42) Yano, H.; Kataoka, M.; Yamashita, H.; Uchida, H.; Watanabe, M. *Langmuir* **2007**, *23*, 6438.

(43) Schulenburg, H.; Muller, E.; Khelashvili, G.; Roser, T.; Bonnemann, H.; Wokaun, A.; Scherer, G. G. *J. Phys. Chem. C* **2009**, *113*, 4069.

(44) Chen, S.; Sheng, W. C.; Yabuuchi, N.; Ferreira, P. J.; Allard, L. F.; Shao-Horn, Y. *J. Phys. Chem. C* **2009**, *113*, 1109.

(45) Yim, W.-L.; Kluner, T. *J. Phys. Chem. C* **2010**, *114*, 7141.

(46) Stamenkovic, V. R.; Mun, B. S.; Mayrhofer, K. J. J.; Ross, P. N.; Markovic, N. M. *J. Am. Chem. Soc.* **2006**, *128*, 8813.

(47) Watanabe, M.; Tsurumi, K.; Mizukami, T.; Nakamura, T.; Stonehart, P. *J. Electrochem. Soc.* **1994**, *141*, 2659.

(48) Wakisaka, M.; Mitsui, S.; Hirose, Y.; Kawashima, K.; Uchida, H.; Watanabe, M. *J. Phys. Chem. B* **2006**, *110*, 23489.

(49) Kobayashi, M.; Hidai, S.; Niwa, H.; Harada, Y.; Oshima, M.; Horikawa, Y.; Tokushima, T.; Shin, S.; Nakamorid, Y.; Aoki, T. *Phys. Chem. Chem. Phys.* **2009**, *11*, 8226.

(50) Krylova, G.; Dimitrijevic, N. M.; Talapin, D. V.; Guest, J. R.; Borchert, H.; Lobo, A.; Rajh, T.; Shevchenko, E. V. *J. Am. Chem. Soc.* **2010**, *132*, 9102.

(51) Toda, T.; Igarashi, H.; Watanabe, M. *J. Electroanal. Chem.* **1999**, *460*, 258.

(52) Fierro, C.; Anderson, A. B.; Scherson, D. A. *J. Phys. Chem. A* **1988**, *92*, 6902.

(53) Liu, H.; Song, C.; Tang, Y.; Zhang, J.; Zhang, J. *Electrochim. Acta* **2007**, *52*, 4532.

(54) Ramirez-Caballero, G. E.; Balbuena, P. B. *J. Phys. Chem. Lett.* **2010**, *1*, 724.

(55) Wiesner, M.; Upert, G.; Angelici, G.; Wennemers, H. *J. Am. Chem. Soc.* **2009**, *132*, 6.

(56) Lang, X. Y.; Guo, H.; Chen, L. Y.; Kudo, A.; Yu, J. S.; Zhang, W.; Inoue, A.; Chen, M. W. *J. Phys. Chem. C* **2010**, *114*, 2600.

(57) Obradovic, M. D.; Grgur, B. N.; Vracar, L. M. *J. Electroanal. Chem.* **2003**, *548*, 69.

(58) Lima, F. H. B.; Ticianelli, E. A. *Electrochim. Acta* **2004**, *49*, 4091.

(59) Kiros, Y. *J. Electrochem. Soc.* **1996**, *143*, 2152.

(60) Xiong, L.; Manthiram, A. *J. Mater. Chem.* **2004**, *14*, 1454.

(61) Yue, Q.; Zhang, K.; Chen, X.; Wang, L.; Zhao, J.; Liu, J.; Jia, J. *Chem. Commun.* **2010**, *46*, 3369.

(62) Wu, J.; Zhang, J.; Peng, Z.; Yang, S.; Wagner, F. T.; Yang, H. *J. Am. Chem. Soc.* **2010**, *132*, 4984.

(63) Yang, H.; Coutanceau, C.; Léger, J.-M.; Alonso-Vante, N.; Lamy, C. *J. Electroanal. Chem.* **2005**, *576*, 305.

(64) He, W.; Wu, X.; Liu, J.; Zhang, K.; Chu, W.; Feng, L.; Hu, X.; Zhou, W.; Xie, S. *J. Phys. Chem. C* **2009**, *113*, 10505.

(65) Kou, R.; Shao, Y.; Wang, D.; Engelhard, M.; Kwak, J.; Wanga, J.; Viswanathan, V. V.; Wang, C.; Lin, Y.; Wang, Y.; Aksay, I. A.; Liu, J. *Electrochem. Commun.* **2009**, *11*, 954.

(66) Hummers, W. S. J.; Offeman, R. E. *J. Am. Chem. Soc.* **1958**, *80*, 1339.

(67) Shih, Y.; Sagar, G.; Lin, S. *J. Phys. Chem. C* **2008**, *112*, 123.

(68) Formo, E.; Lee, E.; Dean, C.; Xia, Y. *Nano Lett.* **2008**, *8*, 668.

(69) Lim, B.; Lu, X.; Jiang, M.; Camargo, P. H. C.; Cho, E.; Lee, E.; Xia, Y. *Nano Lett.* **2008**, *8*, 4043.

(70) Kim, H.; Choi, S.; Nam, S.; Seo, M.; Kim, W. *Catal. Today* **2009**, *146*, 9.

(71) Shukla, A. K.; Raman, R. K.; Choudhury, N. A.; Priolkar, K. R.; Sarode, P. R.; Emura, S.; Kumashiro, R. *J. Electroanal. Chem.* **2004**, *563*, 181.

(72) Santos, L. G. R. A.; Oliveira, C. H. F.; Moraes, I. R.; Ticianelli, E. A. *J. Electroanal. Chem.* **2006**, *596*, 141.

(73) Yang, H.; Vogel, W.; Lamy, C.; Alonso-Vante, N. *J. Phys. Chem. B* **2004**, *108*, 11024.

(74) Stamenkovic, V.; Schmidt, T. J.; Ross, P. N.; Markovic, N. M. *J. Phys. Chem. B* **2002**, *106*, 11970.

(75) Mukerjee, S.; Srinivasan, S.; Soriaga, M. P.; McBreen, J. *J. Phys. Chem.* **1995**, *99*, 4577.

(76) Antoine, O.; Bultel, Y.; Durand, R.; Ozil, P. *Electrochim. Acta* **1998**, *43*, 3681.

(77) Perez, J.; Gonzalez, E. R.; Ticianelli, E. A. *Electrochim. Acta* **1998**, *44*, 1329.

(78) Genies, L.; Faure, R.; Durand, R. *Electrochim. Acta* **1998**, *44*, 1317.

(79) Shukla, A. K.; Neergat, M.; Bera, P.; Jayaram, V.; Hegde, M. S. *J. Electroanal. Chem.* **2001**, *504*, 111–119.

(80) Stamenkovic, V.; Schmidt, T. J.; Ross, P. N.; Markovic, N. M. *J. Electroanal. Chem.* **2003**, *554*, 191.

(81) Kitchin, J. R.; Nørskov, J. K.; Barteau, M. A.; Chen, G. *J. Chem. Phys.* **2004**, *120*, 10240.

(82) Stamenkovic, V. R.; Fowler, B.; Mun, B. S.; Wang, G.; Ross, P. N.; Lucas, C. A.; Markovic, N. M. *Science* **2007**, *315*, 493.

(83) Wang, G.; Gao, Y.; Wang, Z.; Du, C.; Wang, J.; Yin, G. *J. Power Sources* **2010**, *195*, 185.

(84) Deivaraj, T. C.; Chen, W.; Lee, J. *J. Mater. Chem* **2003**, *13*, 2555.

(85) Nishimura, T.; Tsutomu, M.; Masayuki, Y.; Chiaki, I.; Hiroshi, I. *Electrochim. Acta* **2008**, *54*, 499.

(86) Santos, L. G. R. A.; Freitas, K. S.; Ticianelli, E. A. *Electrochim. Acta* **2009**, *54*, 5246.
(87) Chen, W.; Kim, J.; Sun, S. H.; Chen, S. W. *J. Phys. Chem. C* **2008**, *112*, 3891.
(88) Zhang, J.; Vukmirovic, M. B.; Xu, Y.; Mavrikakis, M.; Adzic, R. R. *Angew. Chem., Int. Ed.* **2005**, *44*, 2132.
(89) Stamenkovic, V.; Mun, B. S.; Mayrhofer, K. J. J.; Ross, P. N.; Markovic, N. M.; Rossmeisl, J.; Greeley, J.; Nørskov, J. K. *Angew. Chem., Int. Ed.* **2006**, *45*, 2897.
(90) Appel, M.; Appleby, A. J. *Electrochim. Acta* **1978**, *23*, 1243.
(91) Bron, M.; Bogdanoff, P.; Fiechter, S.; Dorbandt, I.; Hilgendorff, M.; Schulenburg, H.; Tributsch, H. *J. Electroanal. Chem.* **2001**, *500*, 510.
(92) Inaba, M.; Yamada, H.; Tokunaga, J.; Tasaka, A. *Electrochem. Solid-State Lett.* **2004**, *7*, A474.
(93) Arman, B.; Stevens, K.; Vernstrom, G. D.; Atanasoski, R.; Schmoeckel, A. K.; Debeb, M. K.; Dahna, J. R. *Electrochim. Acta* **2007**, *53*, 688.
(94) Bonakdarpour, A.; Delacote, C.; Yang, R.; Wieckowski, A.; Dahn, J. R. *Electrochem. Commun.* **2008**, *10*, 611.
(95) Sarapuu, A.; Vaik, K.; Schiffrin, D. J.; Tammeveski, K. *J. Electroanal. Chem.* **2003**, *541*, 23.
(96) Tammeveski, K.; Kontturi, K.; Nichols, R. J.; Potter, R. J.; Schiffrin, D. J. *J. Electroanal. Chem.* **2001**, *515*, 101.
(97) Kruusenberg, I.; Alexeyeva, N.; Tammeveski, K. *Carbon* **2009**, *47*, 651.
(98) Hossaina, M. S.; Tryka, D.; Yeagera, E. *Electrochim. Acta* **1989**, *34*, 1733.
(99) Yang, H. H.; McCreery, R. L. *J. Electrochem. Soc.* **2000**, *147*, 3420.
(100) Schmidt, T. J.; Stamenkovic, V.; Arenz, M.; Markovic, N. M.; Ross, J. P. N. *Electrochim. Acta* **2002**, *47*, 3765.
(101) Ye, H.; Crooks, R. M. *J. Am. Chem. Soc.* **2007**, *129*, 3627.
(102) Liu, J.; Roussel, C.; Lagger, G.; Tacchini, P.; Girault, H. *Anal. Chem.* **2005**, *77*, 7687.
(103) Ishibashi, K.; Fujishima, A.; Watanabe, T.; Hashimoto, K. *Chem. Commun.* **2000**, *2*, 207.
(104) Kohtani, S.; Yoshida, K.; Maekawa, T.; Iwase, A.; Kudo, A.; Miyabe, H.; Nakagaki, R. *Phys. Chem. Chem. Phys.* **2008**, *10*, 2986.
(105) Liu, J.; Lagger, G.; Tacchini, P.; Girault, H. H. *J. Electroanal. Chem.* **2008**, *619*−*620*, 131.

JP108305V